Virgin Atlantic Net Zero Flight: Final Report

Roger Teoh, Joel Ponsonby, Georgia Gamble, Jonathan Itcovitz & Marc Stettler*

Department of Civil and Environmental Engineering, Imperial College London, SW7 2AZ, United Kingdom

*Corresponding author: m.stettler@imperial.ac.uk

Disclaimer

This is a working paper that represents research in progress. This work has not been peer-reviewed or published by an academic journal and is subject to change.

Summary

Aviation is responsible for 3.5% of the total anthropogenic greenhouse effect, where CO_2 and contrail cirrus collectively account for around 90% of aviation's 2018 global annual mean net effective radiative forcing. On the 28th of November 2023, Virgin Atlantic Flight100 (VS100) achieved a historic milestone as the world's first commercial transatlantic flight powered by 100% sustainable aviation fuel (SAF). The project aims to demonstrate the potential climate benefits of SAF, specifically in reducing both aviation's lifecycle CO_2 emissions and contrail climate forcing. This report details the preparatory efforts conducted to assess specific non-CO_2 pollutants of VS100, namely the aircraft non-volatile particulate matter (nvPM) and contrails, and a subsequent post-analysis of climate forcing resulting from the flight. The key components include: (i) measuring the effects of SAF on aircraft nvPM emissions; (ii) evaluating the models used to simulate the contrail lifecycle and climate forcing; and (iii) comparing the simulated contrail locations with satellite observations.

The simulated mean non-volatile particulate matter (nvPM) number emissions index (EI_n) from VS100 (1.9×10^{14} kg^{-1}) is estimated to be 64% lower relative to an equivalent flight powered by conventional kerosene fuel (5.4×10^{14} kg^{-1}), consistent with the 30–70% reduction in nvPM that was measured before the flight. Simulations in the preparation of VS100 did not predict such formation to occur. This was most likely due to the high cruising altitude of the flight (40,000 feet). Notably, on-board cameras on VS100 did observe the formation of persistent contrails by flights at lower cruising altitudes. The absence of persistent contrails in VS100 and the observation of contrails forming at lower altitudes was consistent with the contrail model forecasts that were made 6 h before the flight. While 58% of the flight distance flown by VS100 satisfied the Schmidt-Appleman criterion that facilitates the formation of short-lived contrails,

geostationary satellite observations failed to detect any short-lived contrails that formed behind the flight trajectory.

1. Introduction

While aviation generates significant socioeconomic benefits globally, it also imposes negative externalities in the form of climate change, noise, and air pollution. Global aviation activity in 2018 is estimated to have accounted for 3.5% of the total human-induced greenhouse effect, Two-thirds of this aviation effect can be attributed to non-CO_2 sources such as contrail cirrus, nitrogen oxides (NO_X), particulate matter and water vapor emissions, while the remaining one-third can be attributed to aviation's CO_2 emissions[1]. More specifically, the two largest components of the global aviation effective radiative forcing (ERF) are contrail cirrus and CO_2 emissions, both of which collectively account for approximately 90% of aviation's total climate forcing in 2018[1].

Contrails are linear-shaped clouds that form behind an aircraft when conditions in the exhaust plume satisfy the Schmidt-Appleman Criterion[2], where the non-volatile particulate matter (nvPM) emitted by the aircraft engines are currently thought to act as a primary source of condensation nuclei for water vapor to condense and subsequently freeze onto in order to form contrail ice crystals[3]. When the atmosphere is supersaturated with respect to ice, these contrails can persist, spread, and mix with other contrails and natural cirrus, transitioning into contrail cirrus with observed lifetimes of up to 19 h and covering up to 10% of the sky (by area) over regions with dense air traffic, such as Europe, the UK, and the US east coast[4,5]. During the day, such clusters of contrail cirrus can reflect incoming solar radiation and contribute to a cooling effect. However, they trap outgoing longwave radiation both during the day and night, resulting in a warming component at all times, and a dominantly warming component at night when there is no incoming solar radiation[6]. According to the current "best-estimates", the 2018 annual mean ERF from contrail cirrus (57.4 [17, 98] mW m^{-2}, 5-95% confidence interval) may be around two times larger than that of aviation's cumulative CO_2 emissions since the 1940s (34.3 [28, 40] mW m^{-2}); there are, however, large uncertainties[1].

The use of sustainable aviation fuel (SAF) potentially offers several co-benefits in reducing aviation's negative externalities. Such benefits include: (i) reductions in CO_2 lifecycle emissions of between 17% and 94%, depending on the feedstock, technology pathway, and energy source used to produce the SAF[7,8]; (ii) reductions in nvPM mass and number emissions resulting from its lower aromatic content and higher fuel hydrogen content[9–11]; (iii) changes to the properties of young contrail that are derived from the nvPM reductions and that result in lower contrail lifetimes and climate forcing[12]; and (iv) improving the air quality in the vicinity of airports[13]. Indeed, measurements from multiple experimental campaigns confirm that use of SAF lowered the nvPM number emissions index (EI_n) by up to 70%[9–11,13,14]. Contrails formed by SAF-burning flights thus tend to have larger contrail ice crystal sizes and lower ice crystal number concentrations and optical depths relative to contrails formed from conventional kerosene fuel under comparable atmospheric conditions[15–17]. Recent simulations, which were informed by these in-situ contrail measurements, suggest that a fleetwide adoption of 100% SAF could reduce the annual mean contrail net radiative forcing (RF) by around 26 – 44%[16,18]. Unlike other mitigation options, such as improvements in aircraft technology and engine fuel efficiency, which could take years or decades to be gradually introduced to the global fleet, SAF that is blended with conventional kerosene can also be safely used in existing aircraft and infrastructure. SAF may also be particularly important for decarbonizing long-haul flights lasting more than 6 hours, which constitute only 5% of all flights globally but contribute to 43% of the annual CO_2 emissions[19], because future disruptive technologies such as electric and liquid hydrogen aircraft will likely lack the required range to complete these long-haul missions.

Given the multiple co-benefits of SAF in mitigating the CO_2 and non-CO_2 effects, Virgin Atlantic established a consortium aimed at showcasing the safety and climate mitigation opportunities associated with SAF. This objective was achieved through the successful operation of Flight100 (VS100) on the 28th of November 2023, the world's first commercial transatlantic flight from London Heathrow (LHR) to New York John F. Kennedy airport (JFK) powered entirely by SAF. This report details the preparatory work and post-analysis of VS100 to assess the contrail cirrus effects resulting from the use of 100% SAF, including:

i. An evaluation of the contrail simulation workflow, including a comparison of model inputs (i.e., flight trajectory and fuel consumption estimates) and model outputs (i.e., simulated contrail location) with data provided by on-board flight data recorders (FDR) and satellites,

ii. A quantification of the effects of SAF and its associated fuel properties on aircraft nvPM emissions,

iii. A review of the historical statistics of the persistent contrail formation and contrail climate forcing for flights travelling from LHR to JFK, and

iv. A post-flight analysis and verification of the CO_2, nvPM and contrail impacts resulting from VS100.

Section 2 describes the materials and methods used to achieve the stated research objectives. Section 3 presents the experimental results approximating the change in aircraft nvPM emissions resulting from the use of 100% SAF, and Section 4 conducts an evaluation of the contrail forecasting workflow by comparing the simulated model outputs with measurements/observations. Section 5 outlines the historical contrail statistics associated with flights travelling from LHR to JFK, while Section 6 conducts a post-analysis of VS100. Finally, Section 7 concludes and summarises the key findings of this report.

2. Materials and Methods

This section outlines the materials and methods used to achieve the stated research objectives. Section 2.1 details the Virgin Atlantic net-zero flight (VS100), while Section 2.2 outlines the datasets and models used to simulate contrails formed along the trajectory of VS100. Section 2.3 describes the experimental measurements that were conducted to quantify the change in aircraft nvPM emissions resulting from the use of SAF. Finally, Section 2.4 outlines the additional datasets used to evaluate the simulated aircraft performance parameters and contrails with measurements and observations.

2.1 Flight100

VS100 was the world's first commercial transatlantic flight to be powered by 100% SAF. The flight, which departed from LHR to JFK on the 28th of November 2023 at 11:30 UTC, was operated on a Boeing 787-900 equipped with two Rolls-Royce Trent 1000 engines. The specific fuel used was a blend of 88% Hydroprocessed Esters and Fatty Acids (HEFA) and 12% Synthetic Aromatic Kerosene (SAK); fuel properties are summarized in Table 1. The fuel hydrogen and aromatics content of the 88% HEFA + 12% SAK blend that was used in VS100 is within the range of previous experimental campaigns[10,11,13,15,20] (Figure 1).

Table 1: Properties of the 88% HEFA + 12% SAK blend that was used on VS100.

Fuel	88% HEFA + 12% SAK blend
Aromatics (vol %)	12.4
Naphthalenes (vol %)	0
Hydrogen content (mass %)	14.54
Specific Energy (MJ/kg)	43.846
Sulphur **Total (mass %)**	< 0.0017

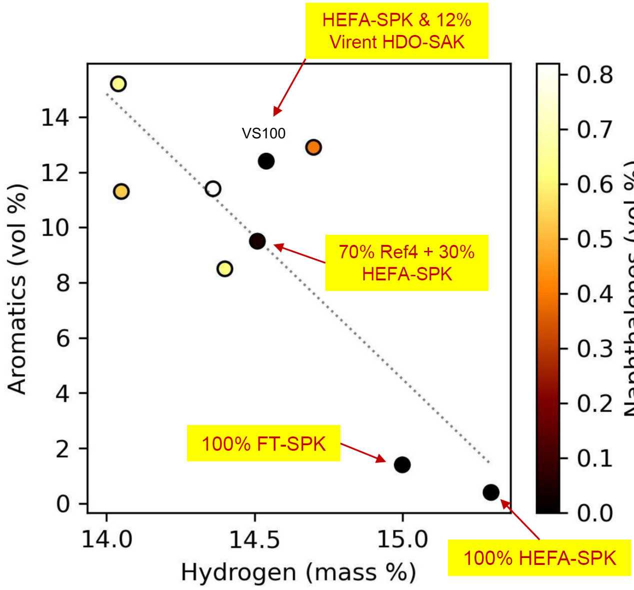

Figure 1: Comparison of the fuel hydrogen and aromatics content used in VS100 (88% HEFA – 12% SAK blend) relative to the SAF that was used in previous experimental campaigns, including the ECLIF II/ND-MAX, NASA ACCESS, EMPAIREX, and AAFEX-II campaigns.

2.2 Contrail simulations

There are several datasets, models, and/or input parameters that are required to simulate contrails formed along a flight trajectory, including:

i. Flight waypoint data, containing the longitude, latitude, altitude, and timestamp, provided at time intervals of between 10 and 300 s, as well as the specific aircraft and engine types,

ii. Aircraft performance models, such as EUROCONTROL's Base of Aircraft Data Family 4 (BADA 4)[21] or the Poll-Schumann (PS) model[22], which provide an estimate of the fuel mass flow rate, aircraft mass, thrust force, and overall efficiency at each flight waypoint,

iii. Historical or forecast 4D meteorological and radiation fields provided by the European Centre for Medium-Range Weather Forecast (ECMWF) ERA5 high-resolution realization (HRES)[23,24], and with corrections applied to the global humidity fields such that the probability density function is consistent with in-situ measurements[25],

iv. The International Civil Aviation Organization (ICAO) Aircraft Engine Emissions Databank (EDB), containing the nvPM emission profile for 178 unique engine types[26], and the T_4/T_2 methodology[19] that uses data from the ICAO EDB to estimate the nvPM EI_n at each flight waypoint, and

v. The state-of-the-art contrail cirrus prediction model (CoCiP)[27,28], which is used to simulate contrail formation, properties, and climate forcing at each flight waypoint.

We note that inputs (i) and (ii) can be either provided directly from FDR or derived from Automatic Dependent Surveillance – Broadcast (ADS-B) telemetry and aircraft performance models (i.e., BADA 4). The former is preferred due to the high frequency of flight waypoint data (once every second), the availability of accurate location data even in regions without ADS-B coverage (i.e., over the oceans), and the availability of true airspeed and fuel mass flow rate data that are directly measured by sensors on-board the aircraft.

For (iv), the ICAO EDB provides the nvPM emissions profile by assuming the use of conventional kerosene fuel. The reduction in nvPM EI_n due to the use of SAF can be estimated as a function of the fuel hydrogen content and engine thrust setting ($\hat{F}$)[18],

$$\Delta\text{nvPM EI}_\text{n}[\%] = \begin{cases} \left(\alpha_0 + \alpha_1 \hat{F}\right) \times \Delta H & \text{, when } \Delta H \leq 0.5\% \\ \left(\alpha_0 + \alpha_1 \hat{F}\right) \times \Delta H \times e^{0.5\times(0.5-\Delta H)} & \text{, when } \Delta H > 0.5\% \end{cases} \tag{1}$$

where $\alpha_0 = -114.21$ and $\alpha_1 = 1.06$ are calibrated coefficients, and ΔH is the arithmetic difference in the fuel hydrogen content between the reference fuel (Jet A-1) and SAF. This adjustment of nvPM EI_n values has been validated by comparison to ground and cruise measurements from four different experimental campaigns[9–11,13,15], where the measured and estimated change in nvPM EI_n are shown to be in good agreement[18].

In our recent study[25], we used the Global Aviation Emissions Inventory based on ADS-B (GAIA)[19], consisting of 103.7 million historical flight trajectories between 2019 and 2021, to simulate contrails globally. The algorithms that were used to perform the global contrail simulation have been open-sourced and can be found via the pycontrails repository in GitHub[29]. For the purposes of this project, we utilize the results from the global contrail simulation[25] to extract historical statistics on persistent contrail formation and contrail climate forcing for all flights that were flown between LHR and JFK. These statistics will serve as a baseline reference for evaluating VS100 (see Section 5).

2.3 nvPM measurements

On the 5th and 6th of October 2023, we conducted an experimental campaign at the Translational Energy Research Centre (TERC) to measure the impact of SAF and engine load conditions on the aircraft nvPM number emissions. The tests used an auxiliary power unit (APU) commonly found in the Boeing 737 and Airbus A320 aircraft. In total, six scenarios were examined, encompassing three different fuel types: 100% Jet A-1, 88% HEFA + 12% SAK blend that was eventually used in VS100 (refer to Section 2.1), and 100% HEFA. For each fuel type, the APU was operated under both "low" ready-to-load (RTL) and "high" full-load (FL) conditions.

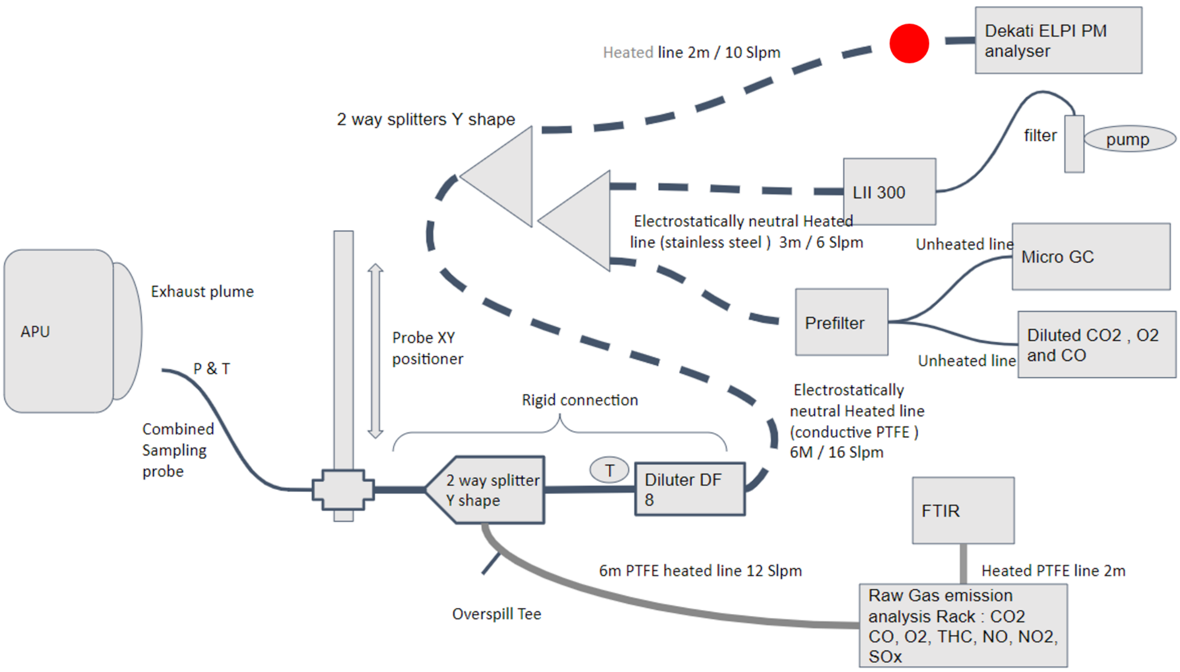

Figure 2: Layout of the TERC sampling system. The equipment used to measure the nvPM particle size distribution (Catalytic stripper, diffusion dryer, SMPS and CPC) can be found on the location of the red marker.

Within the layout of the TERC sampling system used in the experimental campaign (Figure 2), a sampling probe was placed directly behind the APU exhaust, and the nvPM measuring equipment was connected downstream of the exhaust sampling probe by approximately 8 m of heated lines. Volatile material was removed using a catalytic stripper (Catalytic Instruments, CS015) and a diffusion dryer (Cambustion, DD385) was used to reduce the relative humidity of the aerosol flow to less than 28%. Distributions of nvPM particle size were recorded using a scanning mobility particle sizer (SMPS), which comprised a differential mobility analyser (TSI, 3082) and condensation particle counter (TSI, 3756) connected in series. The SMPS was operated with a scan/purge time of 30/15 s and a sheath flow ratio of 1:10. We performed between 3 and 9 scans for each of the six scenarios (3 fuel types and 2 engine load conditions), where the measured particle size distributions were then averaged and fitted with a lognormal size distribution to estimate: (i) nvPM number concentration (N_0); (ii) geometric mean diameter (GMD); and (iii) geometric standard deviation (GSD). We note that particle losses in the catalytic stripper and diffusion dryer have been corrected for in this analysis.

2.4 Evaluation of contrail simulation workflow

To evaluate the datasets and models used in the contrail simulation workflow, we compared:

- flight trajectories provided by on-board FDR versus those derived by ADS-B telemetry,
- simulated persistent contrail formation and advection from CoCiP relative to satellite observations.

An FDR dataset that was provided by Virgin Atlantic was used as a source of "ground truth" in all three of the comparison exercises. The FDR dataset consists of ten unique flights operating from LHR to JFK using the Boeing 787-900 (Table 2). The selection criteria for flights were informed by modelling results from the global contrail simulation[25], where we selected the flight with the largest absolute magnitude of the contrail energy forcing ($EF_{contrail}$) for each quarter in 2020 and 2021.

Table 2: Summary of the ten unique flights where FDR data is provided by Virgin Atlantic.

Flight ID (GAIA)	Flight ID (VIR)	Call sign	Tail number	Rationale
190112-20904-VIR9M	GVYUM_12012019	VIR9M	G-VYUM	Largest $EF_{contrail}$
200813-3355-VIR603	GVOOH_13082020	VIR603	G-VOOH	Smallest $EF_{contrail}$
200320-24530-VIR25B	GVWHO_20032020	VIR25B	G-VWHO	2020 Q1
200606-2048-VIR687	GVNEW_06062020	VIR687	G-VNEW	2020 Q2
200910-35932-VIR603	GVMAP_10092020	VIR603	G-VMAP	2020 Q3
201202-63583-VIR687	GVNEW_02122020	VIR687	G-VNEW	2020 Q4
210117-56447-VIR25B	GVWHO_17012021	VIR25B	G-VWHO	2021 Q1
210626-64072-VIR698	GVOOH_26062021	VIR698	G-VOOH	2021 Q2
210921-36363-VIR3N	GVWOO_21092021	VIR3N	G-VWOO	2021 Q3
211211-83584-VIR9M	GVAAH_11122021	VIR9M	G-VAAH	2021 Q4

The objectives of these comparisons were to understand: (i) the accuracy of the dataset and models used in the contrail simulation workflow; and (ii) the potential errors in the simulated contrail outputs that could arise from alternative data sources, which might be required in the event where FDR data from VS100 becomes unavailable due to unforeseen circumstances. In such a scenario, the trajectory of VS100 would need to be derived from ADS-B telemetry, and an aircraft performance model (BADA 4) would be needed to estimate the fuel consumption and aircraft mass.

The objective of comparing the simulation outputs with satellites was to explore the potential of using these observations to identify the formation/absence of persistent contrails that were formed along the trajectories of the ten unique flights (Table 2), and thus potentially VS100, and to compare the model estimates with these observations. To achieve this, we used satellite imagery provided by the US Geostationary Operational Environmental Satellite (GOES). GOES-16 provides full coverage over the North Atlantic with a spatial resolution of 2 × 2 km and a temporal resolution of every 10 minutes (Figure 3). We detected contrails by using the Advanced Baseline Imager (ABI) imagery, which measures the brightness temperature at different wavelength bands. More specifically, when employing the ash colour scheme, contrails are most clearly distinguished in the brightness temperature differences of 12.0 – 10.8 μm, which results in ice clouds being depicted as dark blue in the image. The accuracy of the simulated persistent contrail formation and advection was then evaluated by superimposing the CoCiP model outputs onto each satellite image.

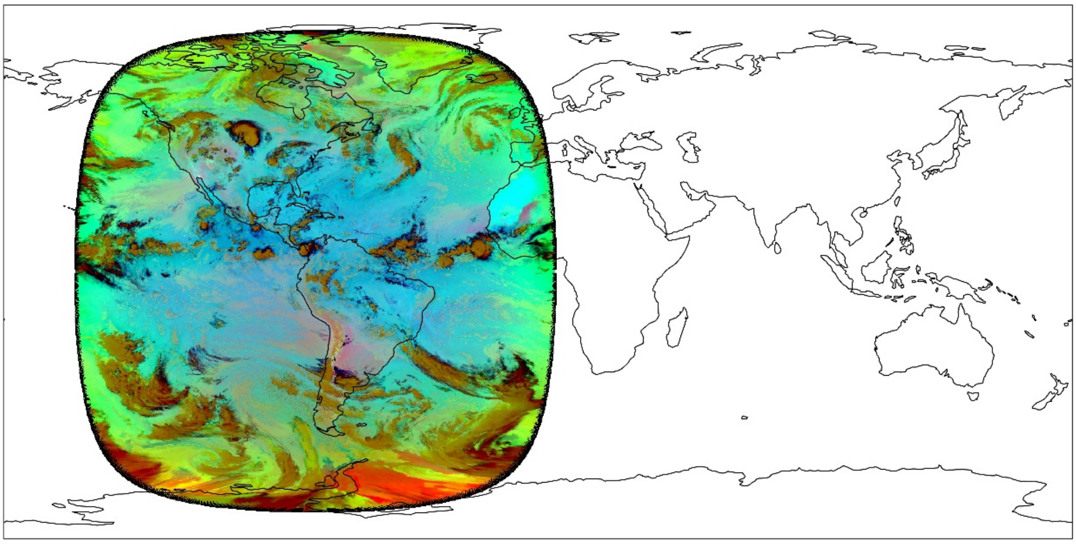

Figure 3: Spatial coverage of the US GOES-16 satellite.

3. SAF effects on aircraft nvPM emissions

In this section, we report the results of the experimental campaign described in Section 2.3, which measured the impact of SAF on the aircraft nvPM emissions. Table 3 provides a summary of the nvPM N_0, GMD, and GSD for each of the six scenarios (3 fuel types and 2 engine load conditions), while Figure 4 show their respective change in nvPM particle size distribution.

Table 3: Lognormal fit parameters for the nvPM particle size distributions under both RTL and FL conditions, including the total nvPM number concentration (N_0), geometric mean diameter (GMD), and geometric standard deviation (GSD).

Fuel and engine load conditions	N_0 (10^6 cm^{-3})		GMD (nm), GSD	
	RTL	FL	RTL	FL
100% Jet A-1	2.70	2.33	27.2, 1.89	29.3, 2.03
88% HEFA + 12% SAK	1.58 (-41%)	1.61 (-31%)	23.0, 1.84	25.2, 2.00
100% HEFA	0.83 (-70%)	0.90 (-61%)	19.8, 1.81	21.8, 1.92

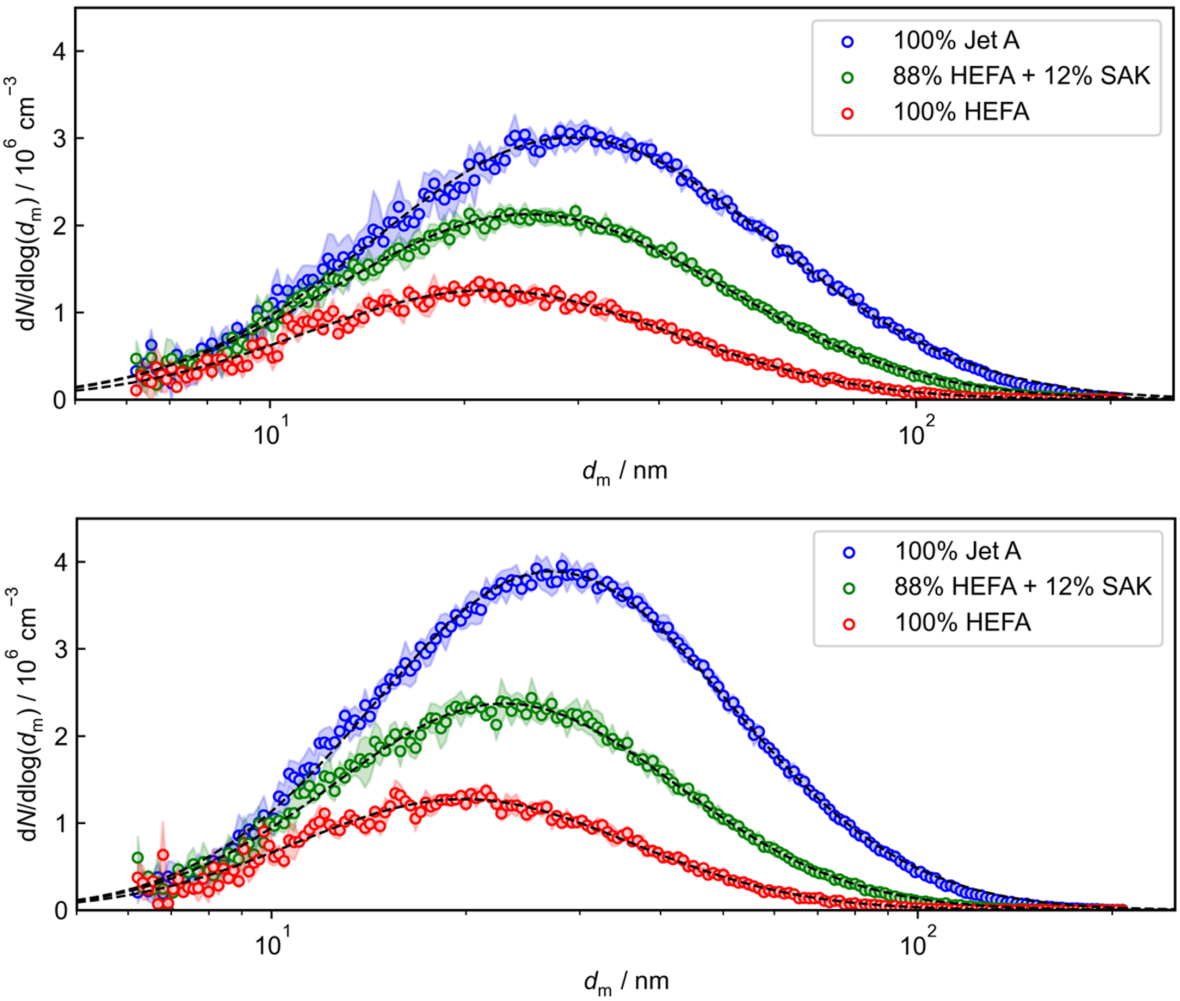

Figure 4: nvPM particle size distribution for the three different fuel types (100% Jet A-1, 88% HEFA + 12% SAK, and 100% HEFA) taken under FL (top) and RTL (bottom) conditions. The data points are fitted with a lognormal distribution, and errors represent the standard deviation taken across at least 3 individual measurements.

Notably, the mean nvPM N_0 for the 88% HEFA-12% SAK blend (1.60 ×10^6 cm^{-3}) was 36% lower than that of the 100% Jet A-1 scenario (2.52 ×10^6 cm^{-3}), with this reduction increasing to 65% when comparing the 100% HEFA (0.87 ×10^6 cm^{-3}) with the 100% Jet A-1. Similarly, the mean GMD was reduced from 28.3 nm for 100% Jet A-1 to 24.1 nm (-15%) for the 88% HEFA + 12% SAK blend, and to 20.8 nm (-26%) for the 100% HEFA. The GSD remained relatively constant, ranging from 1.8 to 2.0 across all six scenarios. On average, the reductions in the nvPM N_0 are more significant in the RTL condition (-41% for the 88% HEFA-12% SAK blend; and -69% for the 100% HEFA relative to 100% Jet A-1) compared to the FL condition (-31% for the 88% HEFA+12% SAK blend; and -61% for the 100% HEFA relative to 100% Jet A-1). These experimental results are consistent with previous studies which found that the percentage reduction in nvPM EI_n: (i) increases with the fuel hydrogen content and decreases with the fuel aromatic content; and (ii) decreases with increasing engine thrust settings[9,13].

4. Comparing model outputs with measurements and observations

In this section, we evaluate the quality of the dataset and model outputs from the contrail simulation workflow with FDR measurements and satellite observations. Section 4.1 compares the flight trajectory provided by on-board FDR with those derived by ADS-B telemetry, while Section 4.2 compares the CoCiP simulated persistent contrails formed by specific flights with observations provided by the GOES-16 satellite.

4.1 Flight trajectories

For 6 out of the 10 flights with FDR data, there are minor discrepancies in the trajectory provided by the FDR versus those derived from ADS-B telemetry (Figure 5). In contrast, for the remaining 4 flights, our comparisons showed significant discrepancies between the FDR and ADS-B derived trajectory (Figure 6). The significant discrepancies for specific flights can most likely be attributed to the intermittent ADS-B satellite coverage of the oceans, which causes the data cleaning algorithm to: (i) perform a great circle interpolation between the known waypoints; and (ii) assume the time where the aircraft performs a step-climb to a new altitude.

We thus compare the simulated persistent contrail length and $EF_{contrail}$ per flight distance between the FDR trajectory and the ADS-B derived trajectory, for which Table 4 summarizes the results for the ten flights with FDR data. We find that the simulations using the FDR trajectory estimate a larger persistent contrail length (Mean of +8.1% with a range of -9.9% to +28.9%) and $EF_{contrail}$ per flight distance (+239 [-28.2, +980] %) relative to the ADS-B derived trajectory. Notably, the discrepancies in the simulated $EF_{contrail}$ per flight distance (+239 [-28.2, +980] %) are significantly larger than in the persistent contrail length (+8.1 [-9.9, +28.9] %) because of error propagation. These results suggest that accurate flight trajectory information is critical in reducing the uncertainty in the simulated formation and climate forcing of persistent contrails.

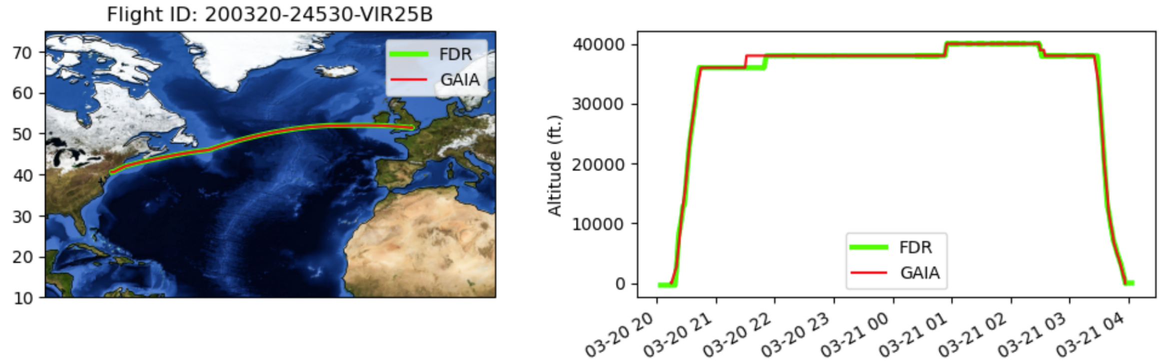

Figure 5: Comparison of an example flight trajectory where there is a good agreement between the FDR-recorded trajectory and the ADS-B trajectory.

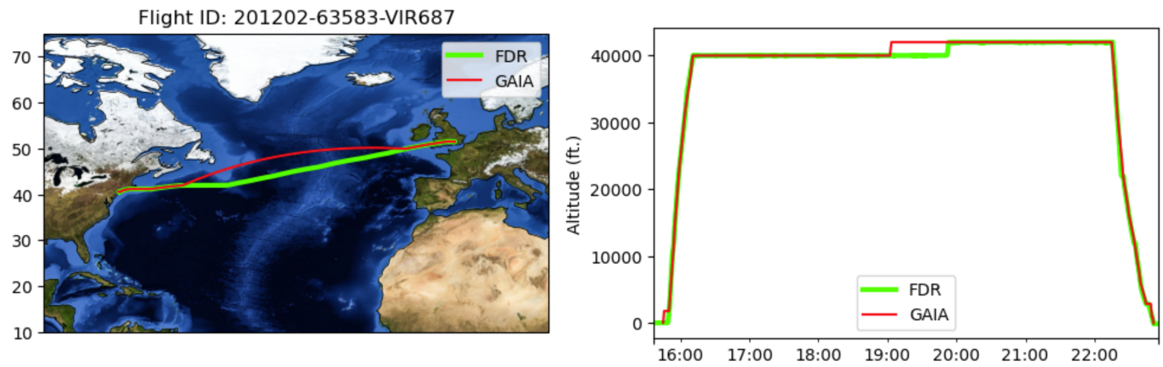

Figure 6: Comparison of an example flight trajectory where there are significant discrepancies between the FDR-recorded trajectory and the ADS-B derived trajectory.

Table 4: Comparison of the simulated persistent contrail length and $EF_{contrail}$ per flight distance between the FDR-recorded trajectory and the ADS-B derived trajectory.

Flight ID (GAIA)	Persistent contrails (km)			$EF_{contrail}$ per flight distance ($\times 10^7$ J m^{-1})		
	FDR	ADS-B	% difference	FDR	ADS-B	% difference
190112-20904-VIR9M	2891	2885	-9.9%	46.9	63.8	+35.9%
200813-3355-VIR603	1337	1329	+13.7%	0.35	-1.55	+349%
200320-24530-VIR25B	2339	2307	+0.8%	9.40	25.2	+169%
200606-2048-VIR687	2186	2209	+19.7%	13.0	17.8	+37.3%
200910-35932-VIR603	3286	3257	+9.7%	0.85	0.92	+980%
201202-63583-VIR687	1990	2088	+4.1%	30.5	38.9	+27.7%
210117-56447-VIR25B	3562	3556	-8.7%	11.7	9.81	-15.8%
210626-64072-VIR698	2226	2175	+28.9%	0.41	3.70	+807%
210921-36363-VIR3N	1332	1286	+17.1%	-1.24	-0.89	-28.2%
211211-83584-VIR9M	2110	2098	+5.6%	12.2	15.3	+26.0%

4.2 Satellite observations

In this analysis, we compare the CoCiP simulated persistent contrails relative to satellite imageries provided by GOES-16. Using the ten flights with FDR data, we identified 13 unique flight segments forming persistent contrails. These persistent contrail segments can be classified into three categories:

i. clear sky conditions without existing contrails and natural cirrus (Figure 7), where persistent contrails observed from satellites can be linked to individual flights,
ii. presence of existing contrail cirrus formed by other flights (Figure 8), thereby making it possible to visually observe the persistent contrail formation but challenging to attribute them to specific flights; and
iii. presence of overlapping natural cirrus (Figure 9), where visual confirmation of persistent contrail formation is not possible.

Table 5 summarises the frequencies of occurrence for each of the three scenarios. For the small number of samples evaluated in this study, only 2 out of the 13 persistent contrails formed under clear sky conditions can be successfully attributed to individual flights. For the remaining 11 out of 13 cases, persistent contrails were formed in the presence of existing contrails and natural cirrus. Despite the challenges in attributing observed persistent contrails to specific flights, a visual comparison between the observations and simulations provide confidence when applying the contrail simulation workflow for VS100 because: (i) CoCiP consistently simulates persistent contrails in regions where contrails and/or natural cirrus were detected by satellites (Figures 8 and 9); and (ii) the simulated contrails tend to sublimate at the time when contrails and/or natural cirrus are dissipating from the satellite imagery.

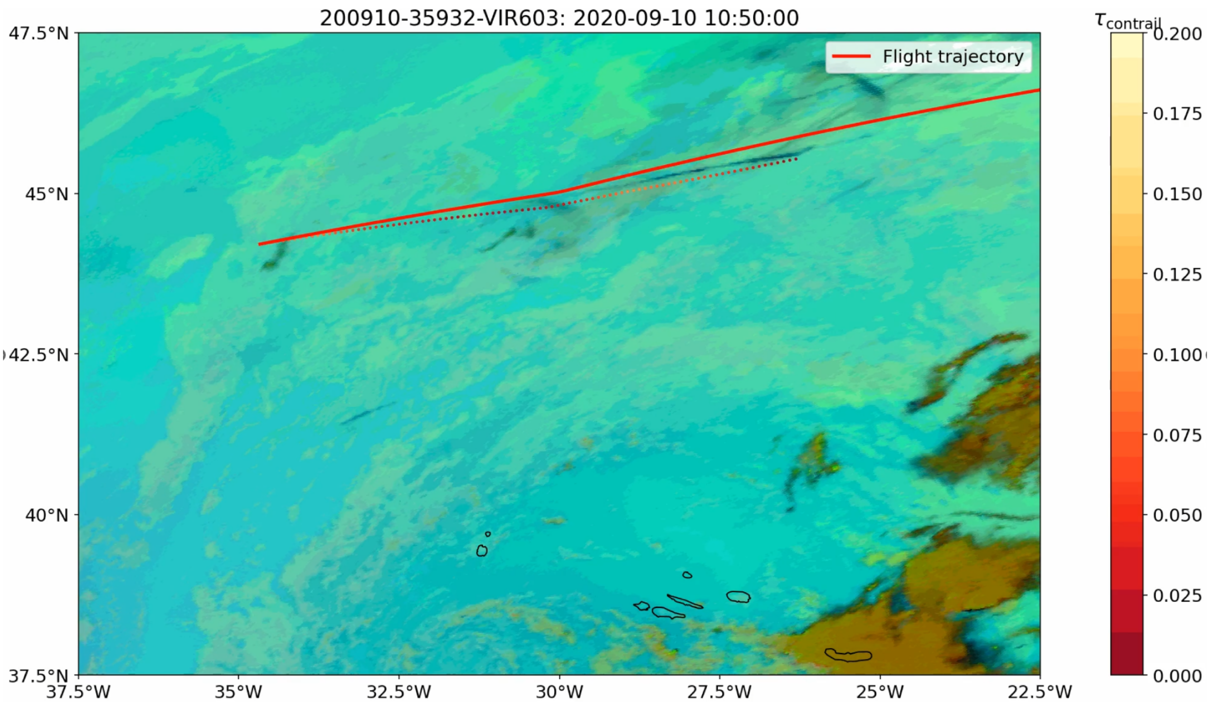

Figure 7: Comparison of the CoCiP simulated persistent contrail formation with satellite images from GOES-16 under clear sky conditions. The flight trajectory is depicted by the red line, and the simulated locations of persistent contrails on the 10th of September 2020 at 10:50:00 UTC are represented by the dotted data points where the contrail optical depth ($\tau_{contrail}$) at each data point is indicated by the colour bar.

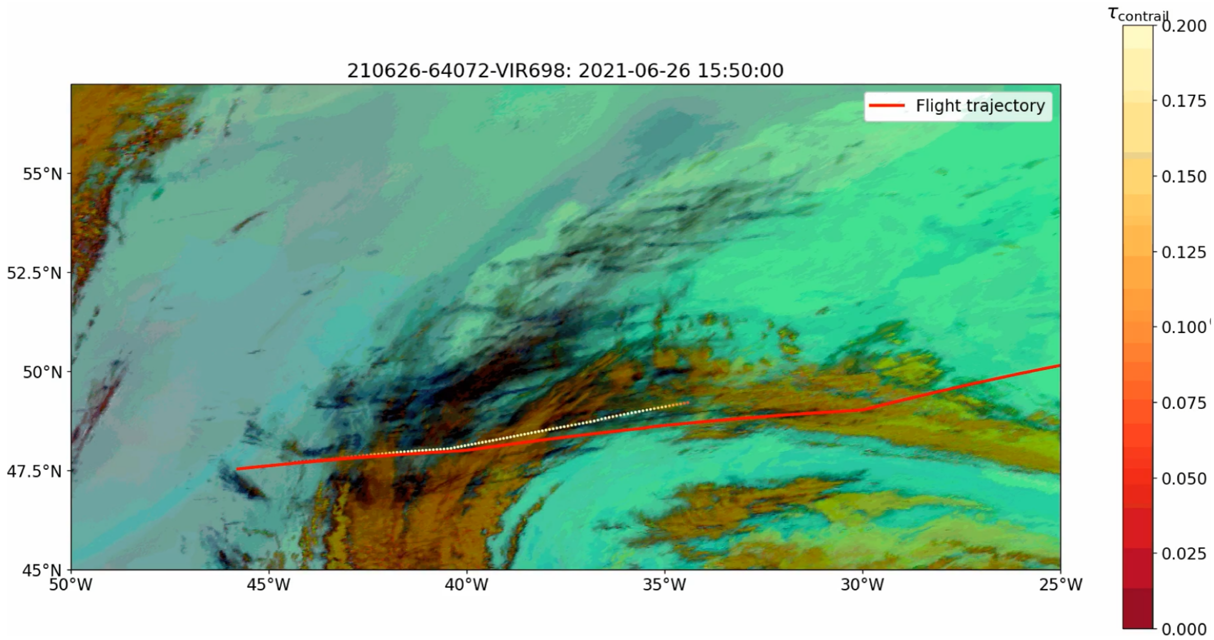

Figure 8: Comparison of the CoCiP simulated persistent contrail formation with satellite images from GOES-16 under the presence of existing contrail cirrus. The flight trajectory is depicted by the red line, and the simulated locations of persistent contrails on the 26th of June 2021 at 15:50:00 UTC are represented by the dotted data points where the contrail optical depth ($\tau_{contrail}$) at each data point is indicated by the colour bar.

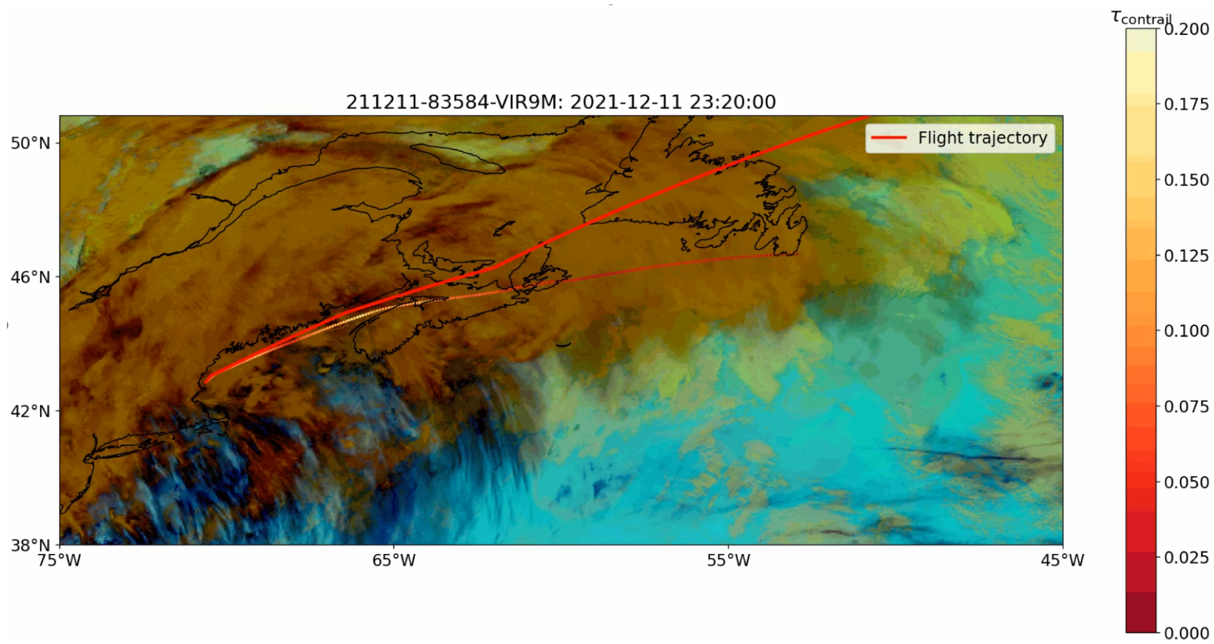

Figure 9: Comparison of the CoCiP simulated persistent contrail formation with satellite images from GOES-16 under the presence of existing contrail cirrus. The flight trajectory is depicted by the red line, and the simulated locations of persistent contrails on the 26th of June 2021 at 15:50:00 UTC are represented by the dotted data points where the contrail optical depth ($\tau_{contrail}$) at each data point is indicated by the colour bar.

Table 5: Classification of the 13 observed persistent contrail segments into three categories (clear sky conditions, presence of existing contrail cirrus, and the presence of overlapping natural cirrus) and the implications of each category in attributing the observed persistent contrails to individual flights.

Scenario	Counts	Description and implications
Clear sky conditions	2	• No/minimal contrails were previously formed along/adjacent to the actual flight trajectory. • Persistent contrails forming under these conditions tend to be < 3 h. • Persistent contrails observed from satellites can be linked to individual flights.
Presence of existing contrail cirrus	6	• Significant contrail cirrus coverage along/adjacent to the actual flight trajectory that were previously formed. • Can visually observe the formation of contrails, but unable to link individual contrails to unique flights.
Presence of overlapping natural cirrus	5	• Significant natural cirrus coverage above/below the region where persistent contrails are expected to form. • Unable to visually confirm the formation of contrails from individual flights.

5. Historical contrail statistics for LHR–JFK

Teoh et al.[25] used the GAIA aviation emissions inventory and CoCiP to simulate contrails globally between 2019 and 2021. Here, we utilised these model outputs, specifically focusing on flights between LHR and JFK, to quantify the historical statistics on persistent contrail formation and climate forcing. The objective of this analysis is to: (i) quantify the range of persistent contrail formation and climate forcing that is expected for flights travelling between LHR and JFK; and (ii) establish a basis for comparison, so that the persistent contrail formation and climate forcing from VS100 can be ranked relative to all other flights.

In total, there were 27,636 unique flights that travelled between LHR and JFK from 2019 to 2021. The main aircraft types used for this route are the Boeing 777 (43.7% of all flights), Boeing 747 (17.1%), Airbus A350 (12.4%), Airbus A330 (10.5%), Airbus A340 (5.7%), Boeing 767 (5.0%), and the Boeing 787 (4.7%). The airline operators between LHR and JFK are British Airways (40.4% of all flights), Virgin Atlantic (32.6%), American Airlines (20.4%), Delta Airlines (5.7%), and JetBlue (0.9%). Around 88% of all analysed flights between LHR and JFK formed persistent contrails lasting for > 5 mins at some point along the flight. For these persistent contrail-forming flights, the mean flight distance forming persistent contrails is 17.1%.

Table 6 breaks down the mean nvPM number per flight distance and $EF_{contrail}$ per flight distance by airline and aircraft type. The results suggest that the Boeing 787-900, which is used for VS100, has the lowest mean $EF_{contrail}$ per flight distance (3.3×10^{7} J m^{-1}) because its nvPM particle number emissions is the lowest (2.9×10^{12} m^{-1}) relative to other aircraft types considered in this analysis. Our earlier study[30], which focused on contrails formed over the North Atlantic, found that a larger nvPM emissions increases the $EF_{contrail}$ per flight distance. This observation can be attributed to the smaller contrail ice crystals formed, which subsequently lowers the ice crystal sedimentation rate and increases the contrail lifetime. Figure 10 classifies the $EF_{contrail}$ per flight distance by westbound and eastbound flights operated by Virgin Atlantic and further segmented by longitude. For eastbound flights, the $EF_{contrail}$ per flight distance trends towards a minimum as it approaches LHR (mean of 1.02 $\times 10^8$ J m^{-1} for waypoints with longitudes > -10°). This value is 71% smaller compared to the mean $EF_{contrail}$ per flight distance for waypoints with longitudes < -10° (3.6 $\times 10^8$ J m^{-1}) because persistent contrails at this flight segment tend to form at dawn. Conversely, westbound flights always exhibit a relatively constant and positive $EF_{contrail}$ per flight distance (mean of 3.4 $\times 10^8$ J m^{-1}). Among this subset of flights between LHR and JFK, 21% of them account for 80% of the total $EF_{contrail}$ on this route.

Several implications emerge when considering these findings in the context of VS100. Firstly, there is a high likelihood of VS100 forming persistent contrails, exceeding an 88% probability. Secondly, in the event where persistent contrails are formed, the mean $EF_{contrail}$ per flight distance for VS100 is more likely to be smaller than the subset of flights considered in this analysis because it is operated by the Boeing 787 and powered by 100% SAF, both of which contributes to a lower relative nvPM emissions. Thirdly, as VS100 will travel in a westbound direction, we do not anticipate specific regions along the flight path where the contrail climate forcing is more likely to be lower-than-average.

Table 6: Mean nvPM number per flight distance and $EF_{contrail}$ per flight distance by airline and aircraft type

Airlines	ICAO aircraft type designator	Mean nvPM number per flight distance ($\times 10^{12}$ m^{-1})	Mean $EF_{contrail}$ per flight distance ($\times 10^7$ J m^{-1})
A	B772	6.78	6.08
	B77W	2.95	4.18
B	B744	8.43	8.34
	B772	6.07	5.85
	B77W	2.78	3.87
C	A333	5.44	5.43
	B764	5.66	5.66
D	A21N	10.7	13.4
Virgin Atlantic	A333	4.49	4.39
	A346	5.89	5.66
	A35K	4.36	4.71

B789	2.93	3.33

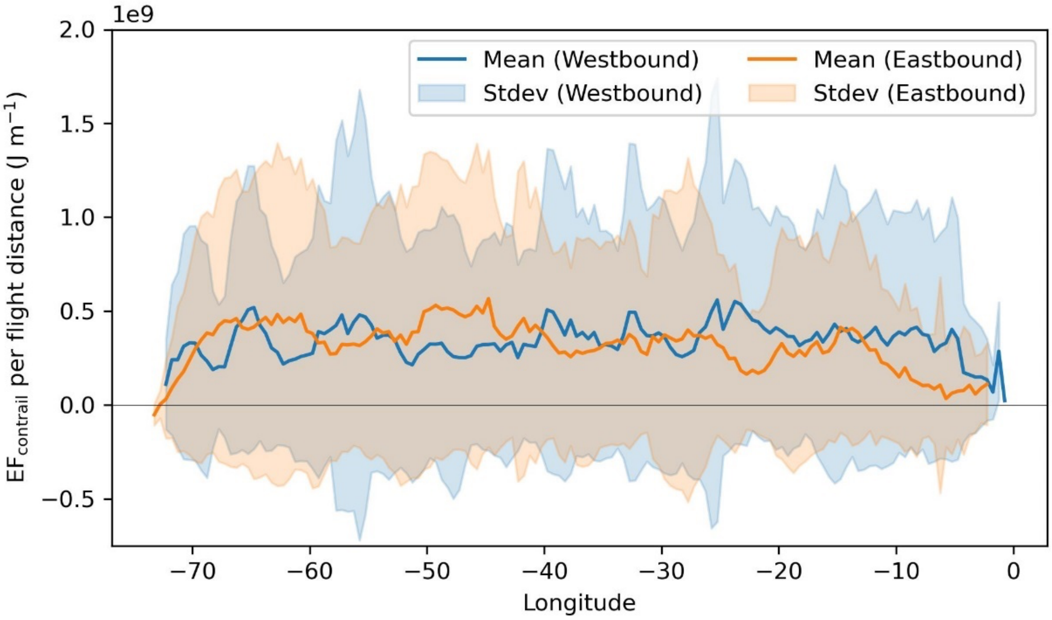

Figure 10: Mean and standard deviation of the $EF_{contrail}$ per flight distance for flights that travelled between LHR and JFK in 2019 – 1021. The data is segmented by westbound (LHR to JFK, blue line) and eastbound (JFK to LHR, orange line) flights, and by longitude.

6. VS100: Post-analysis

The flight plan of VS100 was filed 6 h before the scheduled departure time (11:30:00 UTC on the 28th of November 2023). Notably, this flight operated without revenue-paying passengers or cargo which results in an equivalent passenger load factor of approximately 40%. The aircraft's lower-than-average load factor enabled it to maintain a cruising altitude of FL400 (40,000 feet) throughout the entirety of the flight. Based on the filed trajectory, our contrail forecasts did not predict the formation of persistent contrails throughout the flight (Figure 11).

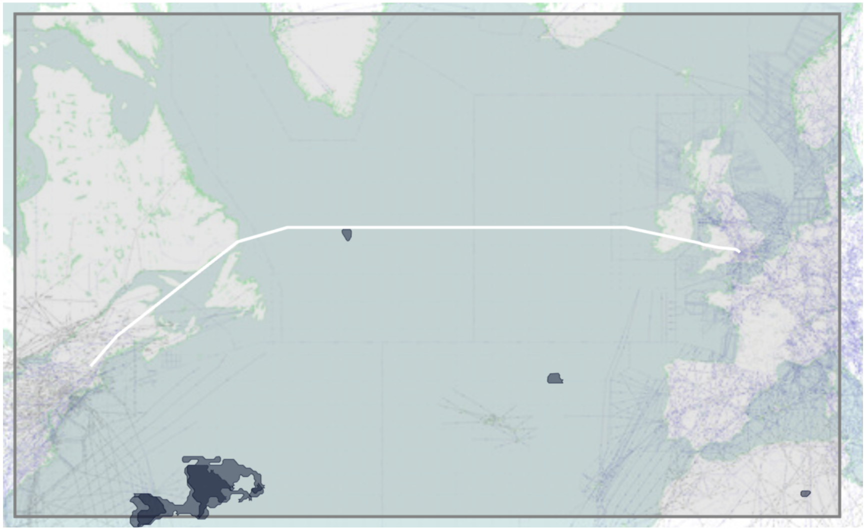

Figure 11: Contrail forecast for the 28th of November 2023, 15:00:00 UTC at FL400. The flight trajectory is depicted by the white line, while the regions that are forecast to form persistent contrails are shown in the shaded region (dark blue).

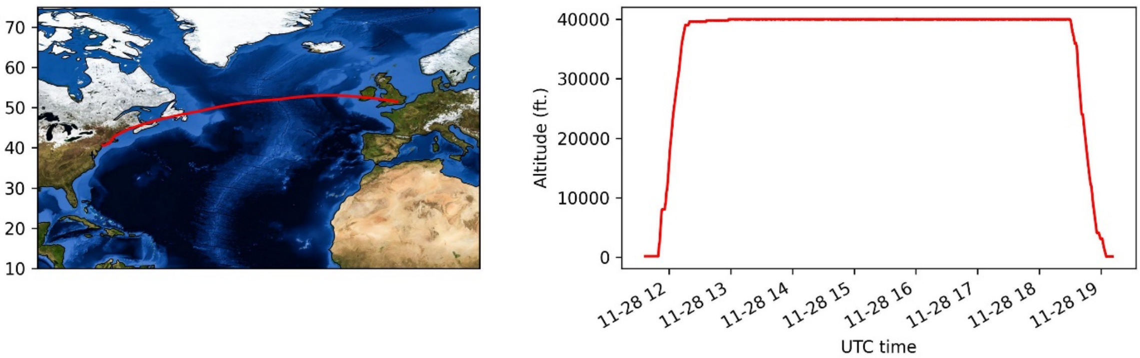

Figure 12: Actual flight trajectory flown by VS100 from London Heathrow to New York John F. Kennedy Airport.

Figure 12 shows the actual flight trajectory that was flown by VS100. The actual flight distance flown by VS100 (5,582 km) was 0.8% longer than the great-circle distance between LHR and JFK (5540 km). Due to the use of 100% SAF, the simulated mean nvPM EI_n from VS100 (1.9 $\times 10^{14}$ kg^{-1}) is estimated to be 64% lower relative to an equivalent flight using Jet A-1 fuel (5.4 $\times 10^{14}$ kg^{-1}).

Using reanalysis (historical) weather data and the contrail simulation workflow, our results suggest that VS100 avoided ice supersaturated regions by maintaining a high cruising altitude of 40,000 feet throughout the entire flight (Figure 13), and as a result, the simulation indicates that no persistent contrails were formed by VS100. Around 58% of the flight distance flown in VS100 (3236 km) satisfied the Schmidt-Appleman Criterion, which could cause the formation of short-lived contrails. However, a visual inspection using satellite observations from GOES-16 did not detect any newly formed contrails close to the trajectory of VS100.

Despite the absence of persistent contrails formed by VS100 and the lack of detection of short-lived contrails in satellite images, on-board cameras captured the formation of persistent contrails by other flights around 16:12:00 UTC, occurring below the cruising altitude of VS100 (Figure 14 (left)). These observations are consistent with the reanalysis weather data, where ice supersaturated regions were predicted below VS100's cruising altitude between 16:00:00 and 16:30:00 UTC (Figure 13). Notably, these persistent contrails observed on-board VS100 were also not detected by satellite images (Figure 14 (right)) likely due to their narrow width and low optical depth, which highlights the limitations of satellites in identifying young contrails and those forming above/below natural cirrus. Nevertheless, faint blue lines can be identified from the satellite images, which supports the occurrence of persistent contrails in this region.

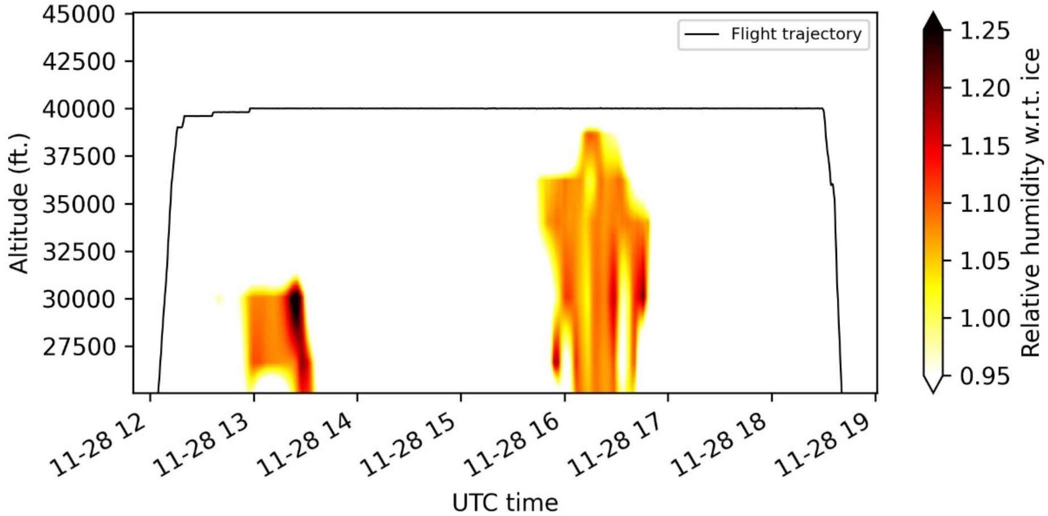

Figure 13: The flight trajectory of VS100 (black line) and the location of ice supersaturated regions along the flight trajectory that was provided by the ECMWF ERA5 HRES reanalysis. The colour bar indicates the relative humidity with respect to ice (RHi) in the ice supersaturated region.

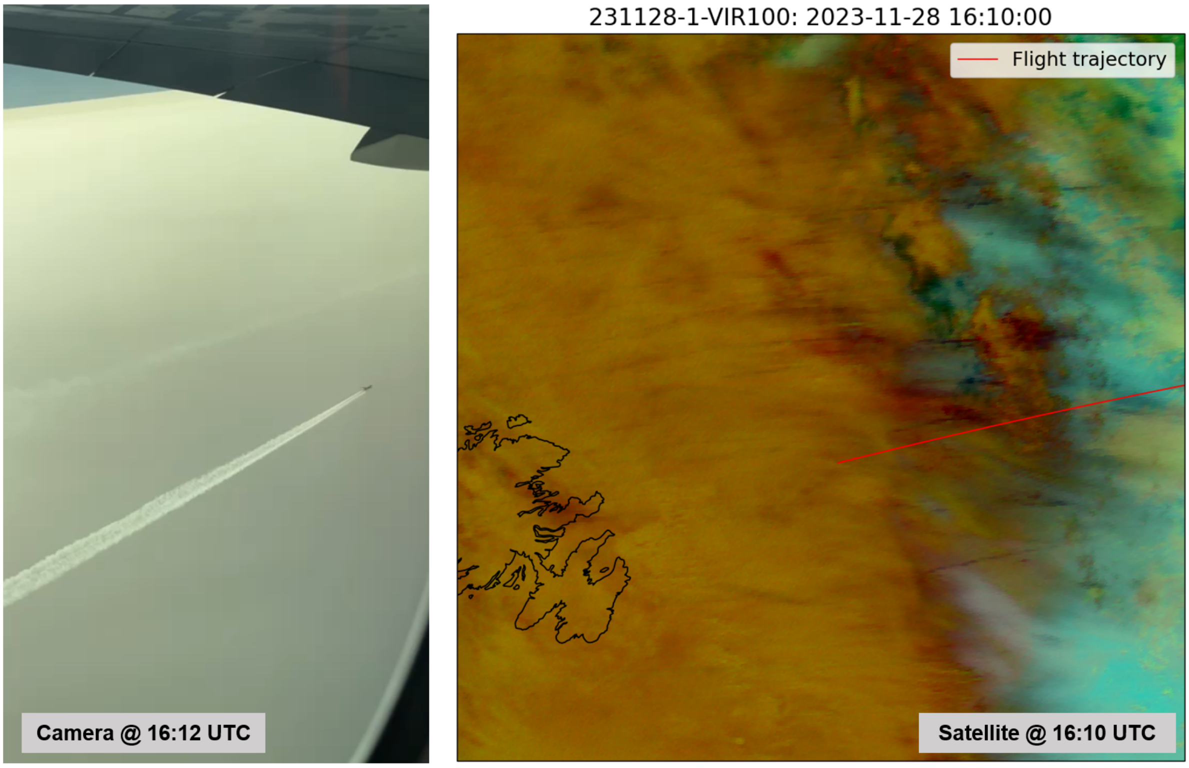

Figure 14: The formation of persistent contrails by other flights that were captured by cameras on-board VS100 at around 16:12:00 UTC (left), and the satellite image from GOES-16 at 16:10:00 UTC (right) which focused on the region where persistent contrail formation was observed.

The absence of persistent contrails formed by VS100, together with the observation of persistent contrails formed by other flights at lower cruising altitudes suggest that current numerical weather prediction models could be capable of predicting the location of ice supersaturated regions. While our sample size remains limited, these findings support the premise that existing contrail forecasts could be utilised to identify flights that are forecast with strongly warming contrails. This, in turn, could facilitate intervention measures such as flight re-routes and a targeted use of SAF to minimise their contrail climate forcing.

7. Conclusions

Aviation emissions consist of CO_2 and non-CO_2 pollutants, both of which are collectively responsible for 3.5% of the total anthropogenic greenhouse effect. The current "best estimate" of the aviation ERF suggests that contrail cirrus is the primary contributor to the overall aviation contrail climate forcing (57.4 [17, 98] mW m^{-2}), followed by its cumulative CO_2 emissions since the 1940s (34.3 [28, 40] mW m^{-2}) and the annual NO_X emissions (17.5 [0.6, 29] mW m^{-2}). SAF is identified as a potential solution to reduce aviation CO_2 lifecycle emissions and contrail climate forcing and can be safely used in existing aircraft engines and infrastructure. To demonstrate the potential climate benefits of SAF, Virgin Atlantic operated the world's first commercial transatlantic flight solely powered by 100% SAF. The flight, identified as Flight100 (VS100), utilized a Boeing 787-900 equipped with the Rolls Royce Trent 1000 engines successfully completed the journey from London to New York on the 28th of November 2023.

This report covered the preparatory work and post-analysis conducted to evaluate nvPM and contrail climate forcing that arise from VS100, including: (i) a quantification of the reduction in nvPM emissions from an APU due to the use of 100% SAF; (ii) evaluation of the datasets and models used in a contrail simulation workflow; and (iii) a comparison of the accuracy of the simulated contrail location and lifetime with satellite observations. In summary, our preparatory work showed that:

- SAF can reduce the nvPM number concentration by 31–70%, depending on the specific fuel properties, SAF blend ratio and engine operating conditions (Section 3),
- Errors in the flight trajectory information tend to propagate and result in large discrepancies in the simulated persistent contrail formation and climate forcing. Accurate flight trajectories with spatiotemporal resolution, such as those derived from FDR instead of ADS-B, should be used to simulate contrails whenever possible (Section 4.1).
- For the limited sample size of 10 unique flights and 13 persistent contrail segments, simulated contrail locations and lifetime were generally consistent with satellite observations. However, the attribution of persistent contrails formed by specific flights is challenging and would only be possible under clear sky conditions without existing contrails and natural cirrus in the vicinity of the flight trajectory (Section 4.3),
- The Boeing 787-900, which was used in VS100, had a lower relative nvPM number emissions, resulting in a lower-than-average mean $EF_{contrail}$ per flight distance among aircraft types commonly used for the LHR-JFK route (Section 5).

The contrail forecasts were evaluated against the filed flight plan of VS100, submitted 6 h before the scheduled departure time (11:30:00 UTC on the 28th of November 2023). The forecasts indicated that persistent contrails were unlikely to form along the designated flight trajectory. FDR data was provided for VS100, and a post-analysis showed that:

- the simulated mean nvPM EI_n (1.9×10^{14} kg^{-1}) was 64% lower than an equivalent flight powered by conventional Jet A-1 fuel (5.4×10^{14} kg^{-1}),
- the flight did not form persistent contrails, which was likely due to its high cruising altitude of 40,000 feet,
- cameras on-board VS100 captured the formation of persistent contrails by other flights cruising below VS100, and these observations were consistent with the ice supersaturated regions provided by the ERA5 HRES reanalysis, and
- no contrails were detected by satellites in the vicinity of the flight trajectory of VS100, even though 58% of the flight distance flown satisfied the Schmidt-Appleman criterion that facilitates the formation of short-lived contrails.

For this flight, the reanalysis weather appears to correctly identify the location of ice supersaturated regions along the trajectory of VS100, which supports the prospect of utilising them for the purposes of contrail climate mitigation. Additionally, VS100 also provides an additional data point that supports the regulatory approval of using 100% SAF with existing aircraft engines. However, the short-term challenge for global aviation would be to significantly scale up the supply of SAF, which currently accounts for less than 0.1% of the global aviation fuel consumption[31], to achieve global widespread SAF adoption and realise its multiple climate benefits.

REFERENCES

1. Lee DS, Fahey DW, Skowron A, et al. The contribution of global aviation to anthropogenic climate forcing for 2000 to 2018. *Atmos Environ*. 2021;244:117834. doi:10.1016/J.ATMOSENV.2020.117834

2. Schumann U. On conditions for contrail formation from aircraft exhausts. *Meteorologische Zeitschrift*. 1996;5:4-23. doi:10.1127/metz/5/1996/4

3. Kärcher B, Yu F. Role of aircraft soot emissions in contrail formation. *Geophys Res Lett*. 2009;36(1):L01804. doi:10.1029/2008GL036649

4. Haywood JM, Allan RP, Bornemann J, et al. A case study of the radiative forcing of persistent contrails evolving into contrail-induced cirrus. *Journal of Geophysical Research: Atmospheres*. 2009;114(D24):D24201. doi:10.1029/2009JD012650

5. Burkhardt U, Kärcher B. Global radiative forcing from contrail cirrus. *Nat Clim Chang*. 2011;1(1):54-58. doi:10.1038/nclimate1068

6. Meerkötter R, Schumann U, Doelling DR, Minnis P, Nakajima T, Tsushima Y. Radiative forcing by contrails. *Ann Geophys*. 1999;17(8):1080-1094. doi:10.1007/s00585-999-1080-7

7. Prussi M, Lee U, Wang M, et al. CORSIA: The first internationally adopted approach to calculate life-cycle GHG emissions for aviation fuels. *Renewable and Sustainable Energy Reviews*. 2021;150:111398. doi:10.1016/J.RSER.2021.111398

8. Andres Gonzalez-Garay, Clara Heuberger-Austin, Xiao Fu, et al. Unravelling the potential of sustainable aviation fuels to decarbonise the aviation sector. *Energy Environ Sci*. Published online 2022. doi:10.1039/D1EE03437E

9. Brem BT, Durdina L, Siegerist F, et al. Effects of Fuel Aromatic Content on Nonvolatile Particulate Emissions of an In-Production Aircraft Gas Turbine. *Environ Sci Technol*. 2015;49(22):13149-13157. doi:10.1021/ACS.EST.5B04167/SUPPL_FILE/ES5B04167_SI_001.PDF

10. Schripp T, Anderson BE, Bauder U, et al. Aircraft engine particulate matter emissions from sustainable aviation fuels: Results from ground-based measurements during the NASA/DLR campaign ECLIF2/ND-MAX. *Fuel*. 2022;325:124764. doi:10.1016/J.FUEL.2022.124764

11. Moore RH, Thornhill KL, Weinzierl B, et al. Biofuel blending reduces particle emissions from aircraft engines at cruise conditions. *Nature*. 2017;543(7645):411-415. doi:10.1038/nature21420

12. Kärcher B. The importance of contrail ice formation for mitigating the climate impact of aviation. *Journal of Geophysical Research: Atmospheres*. 2016;121(7):3497-3505. doi:10.1002/2015JD024696

13. Durdina L, Brem BT, Elser M, Schönenberger D, Siegerist F, Anet JG. Reduction of nonvolatile particulate matter emissions of a commercial turbofan engine at the ground level from the use of a sustainable aviation fuel blend. *Environ Sci Technol*. 2021;55(21):14576-14585. doi:10.1021/ACS.EST.1C04744/SUPPL_FILE/ES1C04744_SI_002.XLSX

14. Schripp T, Anderson B, Crosbie EC, et al. Impact of Alternative Jet Fuels on Engine Exhaust Composition during the 2015 ECLIF Ground-Based Measurements Campaign. *Environ Sci Technol*. 2018;52(8):4969-4978. doi:10.1021/ACS.EST.7B06244/SUPPL_FILE/ES7B06244_SI_001.PDF

15. Voigt C, Kleine J, Sauer D, et al. Cleaner burning aviation fuels can reduce contrail cloudiness. *Communications Earth & Environment 2021 2:1*. 2021;2(1):1-10. doi:10.1038/s43247-021-00174-y

16. Märkl RS, Voigt C, Sauer D, et al. Powering aircraft with 100% sustainable aviation fuel reduces ice crystals in contrails. *EGUsphere*. Published online November 21, 2023:1-37. doi:10.5194/EGUSPHERE-2023-2638

17. Bräuer T, Voigt C, Sauer D, et al. Reduced ice number concentrations in contrails from low aromatic biofuel blends. *Atmos Chem Phys*. 2021;21(22):16817-16826. doi:https://doi.org/10.5194/acp-2021-582

18. Teoh R, Schumann U, Voigt C, et al. Targeted Use of Sustainable Aviation Fuel to Maximise Climate Benefits. *Environ Sci Technol*. 2022;56(23):17246-17255. doi:https://doi.org/10.1021/acs.est.2c05781

19. Teoh R, Engberg Z, Shapiro M, Dray L, Stettler MEJ. A high-resolution Global Aviation emissions Inventory based on ADS-B (GAIA) for 2019 - 2021 [preprint]. *EGUsphere*. Published online 2023. doi:doi.org/10.5194/egusphere-2023-724

20. Moore RH, Shook M, Beyersdorf A, et al. Influence of jet fuel composition on aircraft engine emissions: A synthesis of aerosol emissions data from the NASA APEX, AAFEX, and ACCESS missions. *Energy & Fuels*. 2015;29(4):2591-2600.

21. EUROCONTROL. *User Manual for the Base of Aircraft Data (BADA) Family 4. EEC Technical/Scientific Report No. 12/11/22-58.*; 2016. Accessed August 17, 2021. https://www.eurocontrol.int/model/bada

22. Poll DIA, Schumann U. An estimation method for the fuel burn and other performance characteristics of civil transport aircraft in the cruise. Part 1 fundamental quantities and governing relations for a general atmosphere. *The Aeronautical Journal*. Published online July 20, 2020:1-39. doi:10.1017/aer.2020.62

23. ECMWF. *The Copernicus Programme: Climate Data Store.*; 2021. Accessed February 15, 2022. https://cds.climate.copernicus.eu/#!/home

24. Hersbach H, Bell B, Berrisford P, et al. The ERA5 global reanalysis. *Quarterly Journal of the Royal Meteorological Society*. 2020;146(730):1999-2049. doi:10.1002/qj.3803

25. Teoh R, Engberg Z, Schumann U, et al. Global aviation contrail climate effects from 2019 to 2021 [preprint]. *EGUsphere*. Published online 2023. doi:https://doi.org/10.5194/egusphere-2023-1859

26. EASA. *ICAO Aircraft Engine Emissions Databank (07/2021).*; 2021. Accessed August 17, 2021. https://www.easa.europa.eu/domains/environment/icao-aircraft-engine-emissions-databank

27. Schumann U. A contrail cirrus prediction model. *Geosci Model Dev*. 2012;5(3):543-580. doi:10.5194/gmd-5-543-2012

28. Schumann U, Mayer B, Graf K, Mannstein H. A parametric radiative forcing model for contrail cirrus. *J Appl Meteorol Climatol*. 2012;51(7):1391-1406. doi:10.1175/JAMC-D-11-0242.1

29. Shapiro M, Engberg Z, Teoh R, Dean T. pycontrails: Python library for modeling aviation climate impacts. *Zenodo*. Published online 2023. doi:10.5281/zenodo.7776686

30. Teoh R, Schumann U, Gryspeerdt E, et al. Aviation Contrail Climate Effects in the North Atlantic from 2016-2021. *Atmos Chem Phys*. 2022;22(16):10919-10935. doi:https://doi.org/10.5194/acp-2022-169

31. Bauen A, Bitossi N, German L, Harris A, Leow K. Sustainable Aviation Fuels: Status, challenges and prospects of drop-in liquid fuels, hydrogen and electrification in aviation. *Johnson Matthey Technology Review*. 2020;64(3):263-278. doi:10.1595/205651320X15816756012040